

# UC Berkeley

## UC Berkeley Previously Published Works

### Title

Manipulating Topological Domain Boundaries in the Single-Layer Quantum Spin Hall Insulator 1T'-WSe<sub>2</sub>

### Permalink

<https://escholarship.org/uc/item/3tx562h1>

### Journal

Nano Letters, 19(8)

### ISSN

1530-6984

### Authors

Pedramrazi, Zahra  
Herbig, Charlotte  
Pulkin, Artem  
[et al.](#)

### Publication Date

2019-08-14

### DOI

10.1021/acs.nanolett.9b02157

Peer reviewed

## Manipulating Topological Domain Boundaries in the Single-layer Quantum Spin Hall Insulator $1T'-WSe_2$

Zahra Pedramrazi<sup>1†</sup>, Charlotte Herbig<sup>1†</sup>, Artem Pulkin<sup>2,3†</sup>, Shujie Tang<sup>4,5,6</sup>, Madeleine Philips<sup>7,8</sup>, Dillon Wong<sup>1</sup>, Hyejin Ryu<sup>4,9</sup>, Michele Pizzochero<sup>2</sup>, Yi Chen<sup>1</sup>, Feng Wang<sup>1,10,11</sup>, Eugene J. Mele<sup>7</sup>, Z.X. Shen<sup>5,6</sup>, Sung-Kwan Mo<sup>4</sup>, Oleg V. Yazyev<sup>2,12</sup>, M. F. Crommie<sup>1,10,11</sup>

<sup>1</sup>Department of Physics, University of California at Berkeley, Berkeley, CA 94720, USA.

<sup>2</sup>Institute of Physics, Ecole Polytechnique Fédérale de Lausanne (EPFL), CH-1015 Lausanne, Switzerland.

<sup>3</sup>Division of Chemistry and Chemical Engineering, California Institute of Technology, Pasadena, CA 91125, USA.

<sup>4</sup>Advanced Light Source, Lawrence Berkeley National Laboratory, Berkeley, CA 94720, USA.

<sup>5</sup>Stanford Institute for Materials and Energy Sciences, SLAC National Accelerator Laboratory, Menlo Park, CA 94025, USA.

<sup>6</sup>Geballe Laboratory for Advanced Materials, Departments of Physics and Applied Physics, Stanford University, Stanford, CA 94305, USA.

<sup>7</sup>Department of Physics and Astronomy, University of Pennsylvania, Philadelphia, PA 19104, USA.

<sup>8</sup>Center for Computational Materials Science, Naval Research Laboratory, Washington, D.C. 20375, USA.

<sup>9</sup>Center for Spintronics, Korea Institute of Science and Technology, Seoul 02792, Korea.

<sup>10</sup>Materials Sciences Division, Lawrence Berkeley National Laboratory, Berkeley, CA 94720, USA.

<sup>11</sup>Kavli Energy NanoScience Institute at the University of California Berkeley and the Lawrence Berkeley National Laboratory, Berkeley, CA 94720, USA.

<sup>12</sup>National Centre for Computational Design and Discovery of Novel Materials MARVEL, Ecole Polytechnique Fédérale de Lausanne (EPFL), CH-1015 Lausanne, Switzerland.

† These authors contributed equally to this work.

### Abstract

We report the creation and manipulation of structural phase boundaries in the single-layer quantum spin Hall insulator  $1T'-WSe_2$  by means of scanning tunneling microscope tip pulses. We observe the formation of one-dimensional interfaces between topologically non-trivial  $1T'$  domains having different rotational orientations, as well as induced interfaces between topologically non-trivial  $1T'$  and topologically trivial  $1H$  phases. Scanning tunneling spectroscopy measurements show that  $1T'/1T'$  interface states are localized at domain

1  
2  
3 boundaries, consistent with theoretically predicted unprotected interface modes that form  
4  
5 dispersive bands in and around the energy gap of this quantum spin Hall insulator. We observe a  
6  
7 qualitative difference in the experimental spectral lineshape between topologically “unprotected”  
8  
9 states at 1T'/1T' domain boundaries and protected states at 1T'/1H and 1T'/vacuum boundaries  
10  
11 in single-layer WSe<sub>2</sub>.  
12  
13

14  
15  
16  
17 Keywords: Scanning tunneling microscopy, transition metal dichalcogenides, quantum spin hall  
18  
19 insulators, domain boundary, ferroelasticity.  
20  
21  
22

23  
24 Recent experimental studies have reported the observation of the quantum spin Hall (QSH)  
25  
26 effect in single layers of the transition metal dichalcogenides (TMDs) WTe<sub>2</sub> and WSe<sub>2</sub> in the 1T'  
27  
28 structural phase.<sup>1-5</sup> Evidence of the QSH state include inverted bandgaps,<sup>1</sup> topologically  
29  
30 protected edge states,<sup>1,2,5</sup> as well as quantized edge conduction of  $e^2/h$  per edge.<sup>3,4</sup> QSH edge  
31  
32 states have been observed to reside at 1T'/1H and 1T'/vacuum boundaries, both of which are  
33  
34 interfaces between non-trivial (1T'–TMD) and trivial (1H–TMD phase or vacuum) media.<sup>1,2,5</sup>  
35  
36 Such interfaces are expected to host topologically protected edge states.<sup>6-11</sup> A less well-studied  
37  
38 type of boundary in quantum spin Hall insulator (QSHI) materials is the interface between  
39  
40 different non-trivial domains where the  $Z_2$  topological invariant of the bulk does *not* change  
41  
42 across the interface. We refer to a domain boundary as “topological” when there is a change in  
43  
44 the topological invariant across the interface, and “trivial” when the invariant is the same on  
45  
46 either side of the domain wall. A recent theoretical study of charge transport in quantum Hall  
47  
48 insulators with trivial interfaces predicted that conduction through otherwise dissipationless  
49  
50 quantum Hall edge states can be controllably deflected into trivial interface states, thus enabling  
51  
52 gate-tunable charge and spin transport.<sup>12</sup> Single-layer TMD materials provide a new strategy for  
53  
54  
55  
56  
57  
58  
59  
60

1  
2  
3 constructing such coexisting topological and trivial interfaces by switching the layer structural  
4 phase via some local stimuli.<sup>13-17</sup> For example, the 1T' phase has recently been predicted to be  
5 ferroelastic in single layers, suggesting that it can be switched between different dimerization  
6 orientations by applied stress. This provides a mechanism to induce topologically trivial  
7 interfaces between QSHI domains with different crystallographic orientations. A similar strategy  
8 could allow generation of topologically non-trivial interfaces by inducing local phase switching  
9 between structures that have different  $Z_2$  indices.<sup>18,19</sup>

10  
11 Here we report the local phase manipulation of single-layer 1T'-WSe<sub>2</sub> for the purpose of  
12 creating two kinds of one-dimensional interfaces: (1) trivial interfaces between two 1T' domains  
13 and (2) topological interfaces between 1T' and 1H domains. By using scanning tunneling  
14 microscope (STM) tip pulses we are able to locally switch from the 1T' phase to the 1H phase of  
15 WSe<sub>2</sub>, as well as between different orientations of the 1T' phase. 1T'/1T' domain-boundary  
16 formation is observed to be reversible, supporting the conjecture that single-layer 1T'-WSe<sub>2</sub> is a  
17 ferroelastic material.<sup>18</sup> Our STM measurements show that 1T'/1T' domain boundaries are well-  
18 ordered interfaces that exhibit several different structures. By combining scanning tunneling  
19 spectroscopy (STS) measurements and first-principles calculations we have determined that  
20 1T'/1T' domain boundaries exhibit topologically unprotected one-dimensional (1D) modes that  
21 are dispersive near the Fermi level and that exhibit energy dependent decay lengths. These  
22 modes reside both inside and outside of the 1T'-bulk bandgap and, unlike 1T'/1H interface  
23 modes, do not directly connect bulk valence and conduction bands.

24  
25 Mixed-phase single layers of WSe<sub>2</sub> were grown using molecular beam epitaxy (MBE) on  
26 bilayer graphene (BLG) supported by SiC. These samples exhibit islands that are single domains  
27 of either 1T' or 1H phase, as well as mixed-phase islands with coexisting 1T' and 1H domains.<sup>2</sup>

1  
2  
3 Voltage pulses applied between the STM tip and monolayer  $1T'$ -WSe<sub>2</sub> islands were used to  
4 manipulate the WSe<sub>2</sub> structural phase. Fig. 1 shows STM topographic images of a  $1T'$ -WSe<sub>2</sub>  
5 island before and after application of STM tip pulses. The “before” image (Fig. 1a) shows a  
6 single-domain region of the  $1T'$  phase with a uniform orientation of atomic rows running from  
7 top to bottom (each row contains a zigzag chain of W atoms<sup>1,2,9,11</sup>). Fig. 1b shows the same  
8 region after a voltage pulse of 10 V was applied for 100 ms between the tip and surface at a  
9 constant tip-surface separation of  $\sim 6$  Å. After application of the pulse the island exhibits multiple  
10 domains having different orientations that are connected by ordered 1D domain boundaries (tip  
11 pulses can also cause the formation of adsorbate clusters near domain boundaries, as shown in  
12 Fig. S7).  
13  
14  
15  
16  
17  
18  
19  
20  
21  
22  
23  
24  
25

26 Because the  $1T'$  phase can be formed in three equivalent orientations (via a Peierls  
27 distortion of its  $C_3$ -symmetric  $1T$  parent phase) several possible  $1T'/1T'$  domain boundaries are  
28 expected.<sup>18</sup> The most common  $1T'/1T'$  interface observed in our samples is the  $120^\circ$  domain  
29 boundary which occurs for 85% of all observed boundaries and which connects neighboring  
30 domains rotated with respect to each other by  $120^\circ$  (Fig. 2a). Other observed domain boundaries  
31 are the  $60^\circ$  domain boundary (observed 13% of the time) and the  $0^\circ$  domain boundary (observed  
32 2% of the time), as shown in Figs. 2b, c (structural models are shown in Figs. 2d-f). These well-  
33 ordered interfaces are straight-line defects that extend up to 20 nm in length in our samples. The  
34 formation of  $1T'/1T'$  domain boundaries is reversible through the application of a high current  
35 raster scan by the STM (300mV, 1nA). Such scans remove the adsorbate clusters that form  
36 during the generation of  $1T'/1T'$  domains, likely changing local strain distributions. This  
37 provides additional evidence of the ferroelastic nature of  $1T'$ -WSe<sub>2</sub> (further details are discussed  
38 in section 6 of the SI).  
39  
40  
41  
42  
43  
44  
45  
46  
47  
48  
49  
50  
51  
52  
53  
54  
55  
56  
57  
58  
59  
60

1  
2  
3 The local conversion of single-layer WSe<sub>2</sub> from the 1T' phase to the 1H phase can be  
4 induced using the same voltage pulse method as described above. Fig. 1c shows a different  
5 single-phase 1T' island where the dimer chains run from top to bottom before applying a tip  
6 pulse, while Fig. 1d shows the same region after applying a voltage pulse of 10 V for 100 ms.  
7  
8 The tip pulse causes an extended region of the island to convert into a new phase that exhibits  
9 reduced apparent height. We identified this region as the 1H phase of single-layer WSe<sub>2</sub> (see Fig.  
10 S6 for details). Such 1T' to 1H phase conversion was only observed in “confined” regions as  
11 seen here (i.e. tip-induced 1H domains were always surrounded by other material).  
12  
13  
14  
15  
16  
17  
18  
19  
20  
21

22 While 1T'/1T' domain boundaries could be created by applying tip pulses with  $V_{\text{pulse}} \geq 6$   
23 V, stronger tip pulses ( $V_{\text{pulse}} \geq 10$  V) were required to locally induce the 1T' to 1H phase  
24 transition. These observations agree with predictions that the transition barrier between different  
25 orientations of the 1T' phase should be lower than the barrier for a 1T' → 1H transition.<sup>18</sup> Tip  
26 pulses with  $V_{\text{pulse}} > 6$  V often caused damage to 1T' islands, either by creating holes or by  
27 breaking apart the island. However, once 1T'/1T' and 1T'/1H domain structures are successfully  
28 induced then they remain stable under normal scan conditions.  
29  
30  
31  
32  
33  
34  
35  
36  
37

38 In order to explore the electronic structure of topologically trivial interfaces in a QSHI we  
39 performed STS at the sites of the 120°, 60°, and 0° boundary structures shown in Figs. 2a-c. The  
40  $dI/dV$  spectra obtained in the 1T' bulk (green curves in Figs. 2g-i) reflect the 1T'-WSe<sub>2</sub> bulk  
41 bandgap which has an average full width at half maximum (FWHM) of  $85 \pm 21$  mV centered at  $-$   
42  $130 \pm 5$  mV (determination of the bulk bandgap was performed as described in Supplementary  
43 Note 3 of ref. 2). The spectral weight observed inside the bulk bandgap is explained by lifetime  
44 broadening and the  $-130$  mV offset is due to n-doping induced by the bilayer graphene/SiC  
45 substrate, consistent with previous studies.<sup>2,20,21</sup> The narrow dip at  $V=0$  seen in Figs. 2g-i likely  
46  
47  
48  
49  
50  
51  
52  
53  
54  
55  
56  
57  
58  
59  
60

1  
2  
3 arises from an interplay between disorder and long-range electron-electron interactions as has  
4  
5 been suggested previously.<sup>2,5,20,21,27,28</sup> This feature is more pronounced at 1D domain boundaries  
6  
7 which is consistent with predictions regarding disorder-induced behavior in low dimensions.<sup>28</sup>  
8  
9

10 The spectra for the 120° and 60° domain boundaries (Figs. 2g, h) are similar in that they  
11  
12 both have a minimum at  $V = 0$  and exhibit broad, sloping features in the filled state regime over  
13  
14 the range  $-300 \text{ mV} < V_s < 0$ . Neither of these domain boundaries show any significant signatures  
15  
16 of the bulk bandgap. The 0° domain boundary (Fig. 2i) also has a minimum at  $V = 0$ , but it  
17  
18 shows a pronounced dip right in the bulk bandgap energy range. These experimental features are  
19  
20 qualitatively different from  $dI/dV$  spectra observed at topologically-protected 1T'/vacuum and  
21  
22 1T'/1H boundaries where a clearly defined edge-state peak is seen at the bulk bandgap energy<sup>2</sup> (a  
23  
24 reference  $dI/dV$  spectrum taken at the topological 1T'/vacuum edge is shown in Fig. S8).  
25  
26  
27

28 Because the 120° domain boundaries are the dominant defect feature, we performed a more  
29  
30 in-depth study of their spatially-dependent electronic structure. Fig. 3 shows  $dI/dV$  maps over the  
31  
32 energy range  $-400 \text{ mV} < V_s < 150 \text{ mV}$  for a 120° 1T'/1T' domain boundary that intersects a  
33  
34 1T'/1H domain boundary. The first panel (Fig. 3a) shows an STM topograph of the region and  
35  
36 includes the 120° 1T'/1T' domain boundary (dashed oval) as well as the 1T'/1H boundary  
37  
38 (marked by a vertical dashed line with the 1T' phase to the right). This area allows us to  
39  
40 simultaneously compare the electronic structure of “topological” and “trivial” domain  
41  
42 boundaries.  
43  
44  
45

46 Fig. 3b shows a  $dI/dV$  map measured at  $-400 \text{ mV}$ , which corresponds to an energy below  
47  
48 the lower edge of the bulk 1T'-WSe<sub>2</sub> bandgap shown in Fig. 2g (i.e., the bulk valence states).  
49  
50 Bright intensity corresponding to high LDOS is observed at the site of the 120° domain boundary  
51  
52 while the LDOS near the 1T'/1H interface remains low. Fig. 3c shows a  $dI/dV$  map at  $-120 \text{ mV}$ ,  
53  
54  
55  
56  
57  
58  
59  
60

1  
2  
3 which lies inside the  $1T'$  bulk bandgap. At this energy high LDOS intensity is observed at both  
4 the  $120^\circ$  domain boundary and the  $1T'/1H$  interface region (intensity near the  $1T'/1H$  boundary  
5 originates from the topological edge state.<sup>2</sup> Fig. 3d shows a  $dI/dV$  map measured at  $-60$  mV,  
6 which is near the upper edge of the bulk bandgap. Here high-intensity LDOS is observed near  
7 the  $1T'/1H$  interface (from the topological edge state), while the LDOS at the  $120^\circ$  domain  
8 boundary shows low intensity. Fig. 3e shows a  $dI/dV$  map measured at  $+150$  mV, which  
9 corresponds to an energy well into the bulk conduction band. At this energy neither the  
10 topological  $1T'/1H$  interface state nor the trivial  $120^\circ$  domain boundary show high intensity  
11 features. The high intensity LDOS localized at the  $1T'/1T'$  boundary in the  $dI/dV$  maps indicates  
12 the existence of defect states in the energy range  $-400$  mV  $< V_s < -60$  mV. The broad  
13 spectroscopic feature measured in the  $dI/dV$  point spectrum over this range for  $120^\circ$  domain  
14 boundaries (Fig. 2g) can thus be attributed to confined dispersive defect modes. The  $120^\circ$   
15 domain boundary mode is seen to have a more strongly energy-dependent decay length than the  
16  $1T'/1H$  interface state and to have more intensity at lower energies.

17  
18  
19 In order to clarify the origin of these electronic features, we performed first-principles DFT  
20 simulations. The atomic structure of the interfaces was first relaxed using periodic boundary  
21 conditions in a ribbon geometry with a plane-wave basis set<sup>22</sup> (the relaxed structures are  
22 presented in Figs. 2d-f). We then used the non-equilibrium Green's function method (NEGF) to  
23 model the line defects with semi-infinite boundary conditions.<sup>23,24</sup> The resulting spin-dependent  
24 electronic band structures for the three different interfaces are presented in Figs. 4a-c. The  
25 number of bands, the dispersion, and the spin character of the defect modes changes dramatically  
26 for the different boundary types. Defect modes belonging to the  $60^\circ$  domain boundary (which  
27 has the least amount of symmetry) span the entire bandgap energy region while the localized  
28  
29  
30  
31  
32  
33  
34  
35  
36  
37  
38  
39  
40  
41  
42  
43  
44  
45  
46  
47  
48  
49  
50  
51  
52  
53  
54  
55  
56  
57  
58  
59  
60



1  
2  
3 states of the  $120^\circ$  and  $0^\circ$  domain boundaries do not completely close the bulk energy gap (the  
4  
5 bulk bandgap of the  $60^\circ$  domain boundary model is somewhat affected by the strain that arises  
6  
7 from matching bulk lattice constants with the defect periodicity). We see that while the defect  
8  
9 modes mostly close the overall energy gap for the  $60^\circ$  and  $120^\circ$  domain boundaries, the gap  
10  
11 remains bulk-like for the  $0^\circ$  defect, consistent with our STM spectroscopy observations (Figs.  
12  
13  $2g-i$ ). The simulated  $120^\circ$  domain boundary states are observed to be spin-polarized out of the  
14  
15 plane while for  $60^\circ$  domain boundaries the direction of spin polarization rotates for different  
16  
17 states within the same band (colors in Figs. 4a, b).  $0^\circ$  domain boundaries possess inversion  
18  
19 symmetry and so defect states associated with this boundary show no spin polarization (Fig. 4c).  
20  
21  
22

23  
24 Figs. 4d-f compare the calculated LDOS of the  $120^\circ$ ,  $60^\circ$  and  $0^\circ$  domain boundaries (blue  
25  
26 curves) with the LDOS of the 1T' bulk (grey curves) as a function of energy (the Fermi level has  
27  
28 been shifted to match the experimentally observed n-doping). Overall we find reasonable  
29  
30 agreement between the simulated LDOS in Fig. 4 and the corresponding STM spectroscopy  
31  
32 measurements of Fig. 2. For example, while the experimental bulk bandgap feature vanishes for  
33  
34 the  $60^\circ$  defect (Fig. 2h), an energy gap remains for the  $0^\circ$  defect (Fig. 2i), similar to the theory  
35  
36 plots of Figs. 4e, f. In the  $120^\circ$  case the predicted small 10 meV energy gap is likely smeared out  
37  
38 by level broadening effects that are observed experimentally but not accounted for in  
39  
40 conventional DFT simulations.<sup>25</sup> When we add Gaussian broadening to our calculation then the  
41  
42  $120^\circ$  gap feature is smeared out (Fig. 4d) similar to what is seen experimentally (Fig. 2g). A  
43  
44 significant discrepancy between the theory and the data is the pronounced LDOS peak seen near  
45  
46  $E = 0$  for all three domain boundary types. By contrast, all three domain boundaries show a  
47  
48 broad dip at  $V = 0$  in the STM spectroscopy rather than the predicted peak. This is explained by  
49  
50  
51  
52  
53  
54  
55  
56  
57  
58  
59  
60

1  
2  
3 the coexistence of disorder and electron-electron interactions in these materials which opens a  
4  
5 pseudogap at  $V = 0$  eV but which is not accounted for in DFT simulations.  
6

7  
8 In conclusion, we have successfully manipulated the local electronic and structural  
9  
10 properties of single-layer  $1T'$ -WSe<sub>2</sub>, thereby inducing a local phase transition from the  $1T'$  to  
11  
12 the  $1H$  phase, as well as creating  $1T'/1T'$  domain boundaries. The induced  $1T'/1T'$  domain  
13  
14 boundaries exhibit different rotational configurations, with a  $120^\circ$  domain boundary being the  
15  
16 most common structure. Our combined STS measurements and first-principles calculations show  
17  
18 that these new  $1T'/1T'$  domain boundaries yield topologically unprotected 1D states that are  
19  
20 dispersive in energy near the Fermi level and exhibit energy-dependent decay lengths. These  
21  
22 results create new opportunities for exploring electron- and spin-based devices where charge  
23  
24 carriers traveling along QSH edges might be deflected into trivial domain boundary modes in a  
25  
26 controllable fashion.<sup>12</sup>  
27  
28  
29  
30  
31  
32

### 33 ACKNOWLEDGEMENT

34  
35 This research was supported as part of the Center for Novel Pathways to Quantum  
36  
37 Coherence in Materials, an Energy Frontier Research Center funded by the U.S. Department of  
38  
39 Energy, Office of Science, Basic Energy Sciences (STM spectroscopy and dI/dV mapping).  
40  
41 Support was also provided by the VdW Heterostructure program (KCWF16) (surface preparation  
42  
43 and topographic characterization) funded by the Director, Office of Science, Office of Basic  
44  
45 Energy Sciences, Materials Sciences and Engineering Division, of the US Department of Energy  
46  
47 under Contract No. DE-AC02-05CH11231 and by the National Science Foundation under award  
48  
49 EFMA-1542741 (local phase transition generation). The work performed at the ALS (film  
50  
51 characterization) was supported by the Office of Basic Energy Sciences, US DOE under Contract  
52  
53  
54  
55  
56  
57  
58  
59  
60

1  
2  
3 No. DE-AC02-05CH11231. C. H. acknowledges the support of Alexander von Humboldt  
4  
5 Foundation for a Feodor Lynen research fellowship. The work performed at the Stanford  
6  
7 Institute for Materials and Energy Sciences and Stanford University (MBE growth) was  
8  
9 supported by the Division of Materials Science, Office of Basic Energy Sciences, US DOE under  
10  
11 contract No. DE-AC02-76SF00515. Theoretical modeling of the two-channel conductance by  
12  
13 M.P. and E.J.M. was supported by the DOE Office of Basic Energy Sciences under grant DE-  
14  
15 FG02-ER45118. M.P. acknowledges support from an NRC Research Associateship award at the  
16  
17 U.S. Naval Research Laboratory. S. T. acknowledges the support from the CPSF-CAS Joint  
18  
19 Foundation for Excellent Postdoctoral Fellows. H. R. acknowledges fellowship support from  
20  
21 NRF, Korea through Max Planck Korea/POSTECH Research Initiative No.  
22  
23 2016K1A4A4A01922028. A.P., M.P., and O.V.Y. acknowledge support by the ERC Starting  
24  
25 grant “TopoMat” (Grant No. 306504) (ab initio theoretical formalism development), as well as  
26  
27 Swiss National Science Foundation grants No. 162612 (2D bulk electronic structure) and No.  
28  
29 172543 (1D interface electronic structure). First-principles calculations were performed at the  
30  
31 Swiss National Supercomputing Centre (CSCS) under project s832 and the facilities of Scientific  
32  
33 IT and Application Support Center of EPFL. We thank Quansheng Wu for assistance with  
34  
35 calculations, and we want to thank Canxun Zhang with helpful discussion.  
36  
37  
38  
39  
40  
41  
42  
43  
44  
45  
46  
47  
48  
49

## 50 REFERENCES

- 51  
52 1 S. Tang, C. Zhang, D. Wong, Z. Pedramrazi, H. Z. Tsai, C. Jia, B. Moritz, M. Claassen,  
53 H. Ryu, S. Kahn, J. Jiang, H. Yan, M. Hashimoto, D. Lu, R. G. Moore, C. C. Hwang, C.  
54 Hwang, Z. Hussain, Y. Chen, M. M. Ugeda, Z. Liu, X. Xie, T. P. Devereaux, M. F.  
55  
56  
57  
58  
59  
60

- 1  
2  
3 Crommie, S.-K. Mo, Z. X. Shen, Quantum spin Hall state in monolayer 1T'-WTe<sub>2</sub>.  
4 Nature Physics **13**, 683, (2017).  
5  
6 2 M. M. Ugeda, A. Pulkin, S. Tang, H. Ryu, Q. Wu, Y. Zhang, D. Wong, Z. Pedramrazi, A.  
7 Martín-Recio, Y. Chen, F. Wang, Z. X. Shen, S.-K. Mo, O. V. Yazyev, M. F. Crommie,  
8 Observation of topologically protected states at crystalline phase boundaries in single-  
9 layer WSe<sub>2</sub>. Nature Communications **9**, 3401, (2018).  
10  
11 3 S. Wu, V. Fatemi, Q. D. Gibson, K. Watanabe, T. Taniguchi, R. J. Cava, P. Jarillo-  
12 Herrero, Observation of the quantum spin Hall effect up to 100 Kelvin in a monolayer  
13 crystal. Science **359**, 76, (2018).  
14  
15 4 Z. Fei, T. Palomaki, S. Wu, W. Zhao, X. Cai, B. Sun, P. Nguyen, J. Finney, X. Xu, D.  
16 Cobden, Edge conduction in monolayer WTe<sub>2</sub>. Nature Physics **13**, 677, (2017).  
17  
18 5 Z.-Y. Jia, Y.-H. Song, X.-B. Li, K. Ran, P. Lu, H.-J. Zheng, X.-Y. Zhu, Z.-Q. Shi, J. Sun,  
19 J. Wen, D. Xing, S.-C. Li, Direct visualization of a two-dimensional topological insulator  
20 in the single-layer 1T'-WTe<sub>2</sub>. *Physical Review B* **96**, 041108, (2017).  
21  
22 6 C. L. Kane, E. J. Mele, Quantum Spin Hall Effect in Graphene. *Physical Review Letters*  
23 **95**, 226801, (2005).  
24  
25 7 B. A. Bernevig, S.-C. Zhang, Quantum Spin Hall Effect. *Physical Review Letters* **96**,  
26 106802, (2006).  
27  
28 8 M. Z. Hasan, C. L. Kane, Colloquium: Topological insulators. *Reviews of Modern*  
29 *Physics* **82**, 3045, (2010).  
30  
31 9 X. Qian, J. Liu, L. Fu, J. Li, Quantum spin Hall effect in two-dimensional transition  
32 metal dichalcogenides. *Science* **346**, 1344, (2014).  
33  
34 10 Y. Ma, L. Kou, X. Li, Y. Dai, S. C. Smith, T. Heine, Quantum spin Hall effect and  
35 topological phase transition in two-dimensional square transition-metal dichalcogenides.  
36 *Physical Review B* **92**, 085427, (2015).  
37  
38 11 D.-H. Choe, H.-J. Sung, K. J. Chang, Understanding topological phase transition in  
39 monolayer transition metal dichalcogenides. *Physical Review B* **93**, 125109, (2016).  
40  
41 12 M. Phillips, E. J. Mele, Charge and spin transport on graphene grain boundaries in a  
42 quantizing magnetic field. *Physical Review B* **96**, 041403, (2017).  
43  
44 13 Y. Wang, J. Xiao, H. Zhu, Y. Li, Y. Alsaied, K. Y. Fong, Y. Zhou, S. Wang, W. Shi, Y.  
45 Wang, A. Zettl, E. J. Reed, X. Zhang, Structural phase transition in monolayer MoTe<sub>2</sub>  
46 driven by electrostatic doping. Nature **550**, 487, (2017).  
47  
48 14 Y.-C. Lin, D. O. Dumcenco, Y.-S. Huang, K. Suenaga, Atomic mechanism of the  
49 semiconducting-to-metallic phase transition in single-layered MoS<sub>2</sub>. *Nature*  
50 *Nanotechnology* **9**, 391, (2014).  
51  
52 15 D. H. Keum, S. Cho, J. H. Kim, D.-H. Choe, H.-J. Sung, M. Kan, H. Kang, J.-Y. Hwang,  
53 S. W. Kim, H. Yang, K. J. Chang, Y. H. Lee, Bandgap opening in few-layered  
54 monoclinic MoTe<sub>2</sub>. *Nature Physics* **11**, 482, (2015).  
55  
56 16 R. Kappera, D. Voiry, S. E. Yalcin, B. Branch, G. Gupta, A. D. Mohite, M. Chhowalla,  
57 Phase-engineered low-resistance contacts for ultrathin MoS<sub>2</sub> transistors. *Nature*  
58 *Materials* **13**, 1128, (2014).  
59  
60

- 1  
2  
3  
4  
5  
6  
7  
8  
9  
10  
11  
12  
13  
14  
15  
16  
17  
18  
19  
20  
21  
22  
23  
24  
25  
26  
27  
28  
29  
30  
31  
32  
33  
34  
35  
36  
37  
38  
39  
40  
41  
42  
43  
44  
45  
46  
47  
48  
49  
50  
51  
52  
53  
54  
55  
56  
57  
58  
59  
60
- 17 Y. Li, K.-A. N. Duerloo, K. Wauson, E. J. Reed, Structural semiconductor-to-semimetal phase transition in two-dimensional materials induced by electrostatic gating. *Nature Communications* **7**, 10671, (2016).
- 18 W. Li, J. Li, Ferroelasticity and domain physics in two-dimensional transition metal dichalcogenide monolayers. *Nature Communications* **7**, 10843, (2016).
- 19 K.-A. N. Duerloo, Y. Li, E. J. Reed, Structural phase transitions in two-dimensional Mo- and W-dichalcogenide monolayers. *Nature Communications* **5**, 4214, (2014).
- 20 Y.-H. Song, Z.-Y. Jia, D. Zhang, X.-Y. Zhu, Z.-Q. Shi, H. Wang, L. Zhu, Q.-Q. Yuan, H. Zhang, D.-Y. Xing, S.-C. Li, Observation of Coulomb gap in the quantum spin Hall candidate single-layer 1T'-WTe<sub>2</sub>. *Nature Communications* **9**, 4071, (2018).
- 21 J. G. Massey, M. Lee, Direct Observation of the Coulomb Correlation Gap in a Nonmetallic Semiconductor, Si: B. *Physical Review Letters* **75**, 4266, (1995).
- 22 P. Giannozzi, S. Baroni, N. Bonini, M. Calandra, R. Car, C. Cavazzoni, D. Ceresoli, G. L. Chiarotti, M. Cococcioni, I. Dabo, A. Dal Corso, S. D. Gironcoli, S. Fabris, G. Fratesi, R. Gebauer, U. Gerstmann, C. Gougoussis, A. Kokalj, M. Lazzeri, L. Martin-Samos, N. Marzari, F. Mauri, R. Mazzarello, S. Paolini, A. Pasquarello, L. Paulatto, C. Sbraccia, S. Scandolo, G. Sclauzero, A. P. Seitsonen, A. Smogunov, P. Umari, R. M. Wentzcovitch, QUANTUM ESPRESSO: a modular and open-source software project for quantum simulations of materials. *Journal of Physics: Condensed Matter* **21**, 395502, (2009).
- 23 T. Ozaki, Variationally optimized atomic orbitals for large-scale electronic structures. *Physical Review B* **67**, 155108, (2003).
- 24 T. Ozaki, H. Kino, Numerical atomic basis orbitals from H to Kr. *Physical Review B* **69**, 195113, (2004).
- 25 V. W. Brar, S. Wickenburg, M. Panlasigui, C.-H. Park, T. O. Wehling, Y. Zhang, R. Decker, Ç. Girit, A. V. Balatsky, S. G. Louie, A. Zettl, M. F. Crommie, Observation of Carrier-Density-Dependent Many-Body Effects in Graphene via Tunneling Spectroscopy. *Physical Review Letters* **104**, 036805, (2010).
- 26 Y. A. Bychkov, E. I. Rashba, Properties of a 2D electron gas with a lifted spectrum degeneracy. *Phys. -JETP Lett.* **39**, 78, (1984).
- 27 B. L. Altshuler & A. G. Aronov, Zero bias anomaly in tunnel resistance and electron-electron interaction. *Solid State Commun.* **30**, 115, (1979).
- 28 L. Bartosch & P. Kopietz, Zero bias anomaly in the density of states of low-dimensional metals. *Eur. Phys. J. B* **28**, 29, (2002)

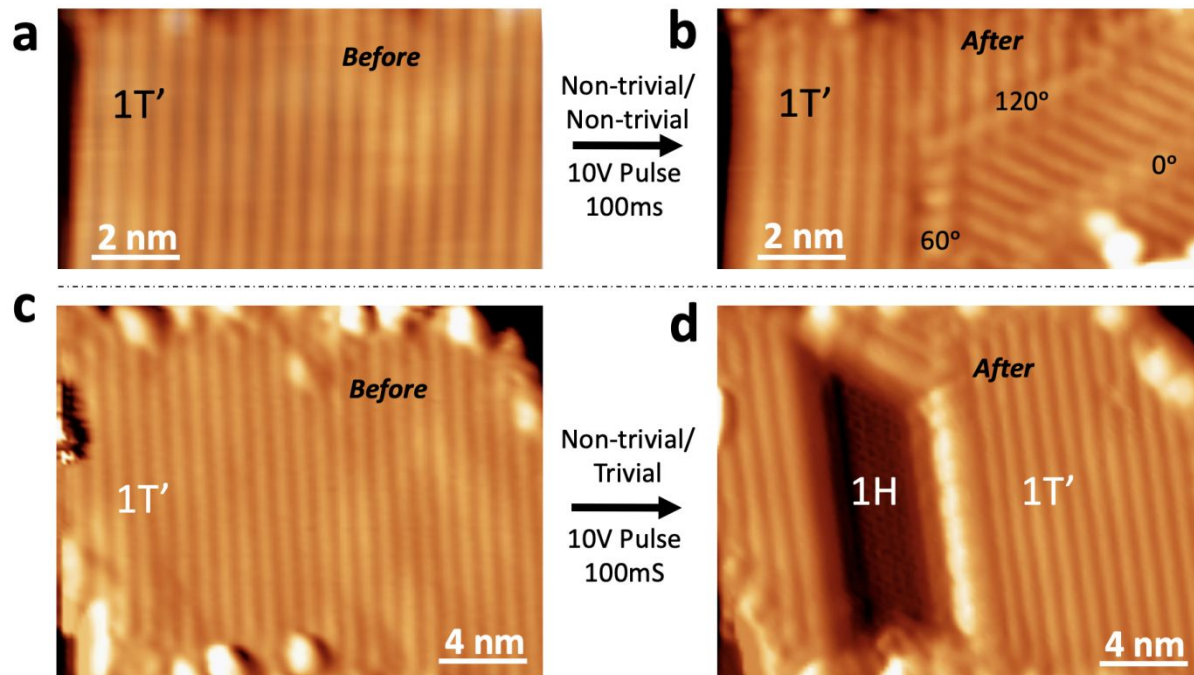


**Figure 1: STM tip-induced structural change in monolayer 1T'-WSe<sub>2</sub>.** STM topographic images of a monolayer 1T'-WSe<sub>2</sub> island (a) before and (b) after applying a tip voltage pulse ( $V_{\text{pulse}} = 10 \text{ V}$ ,  $\Delta t = 100 \text{ ms}$ , tip-surface separation =  $6 \text{ \AA}$ ). The tip pulse creates 1T'/1T' domain boundaries having different rotational orientations. STM topographic images show a different island (c) before and (d) after an applied tip voltage pulse ( $V_{\text{pulse}} = 10 \text{ V}$ ,  $\Delta t = 100 \text{ ms}$ , tip-surface separation =  $6 \text{ \AA}$ ) induces a 1T' to 1H structural phase transition near the center of the island.  $V_s = 1 \text{ V}$ ,  $I_t = 10 \text{ pA}$ ,  $T = 4.5 \text{ K}$  for all images. (Image intensity here is proportional to  $dz/dx$  (where  $z$  is height) in order to enhance contrast between regions having different structural phases.)

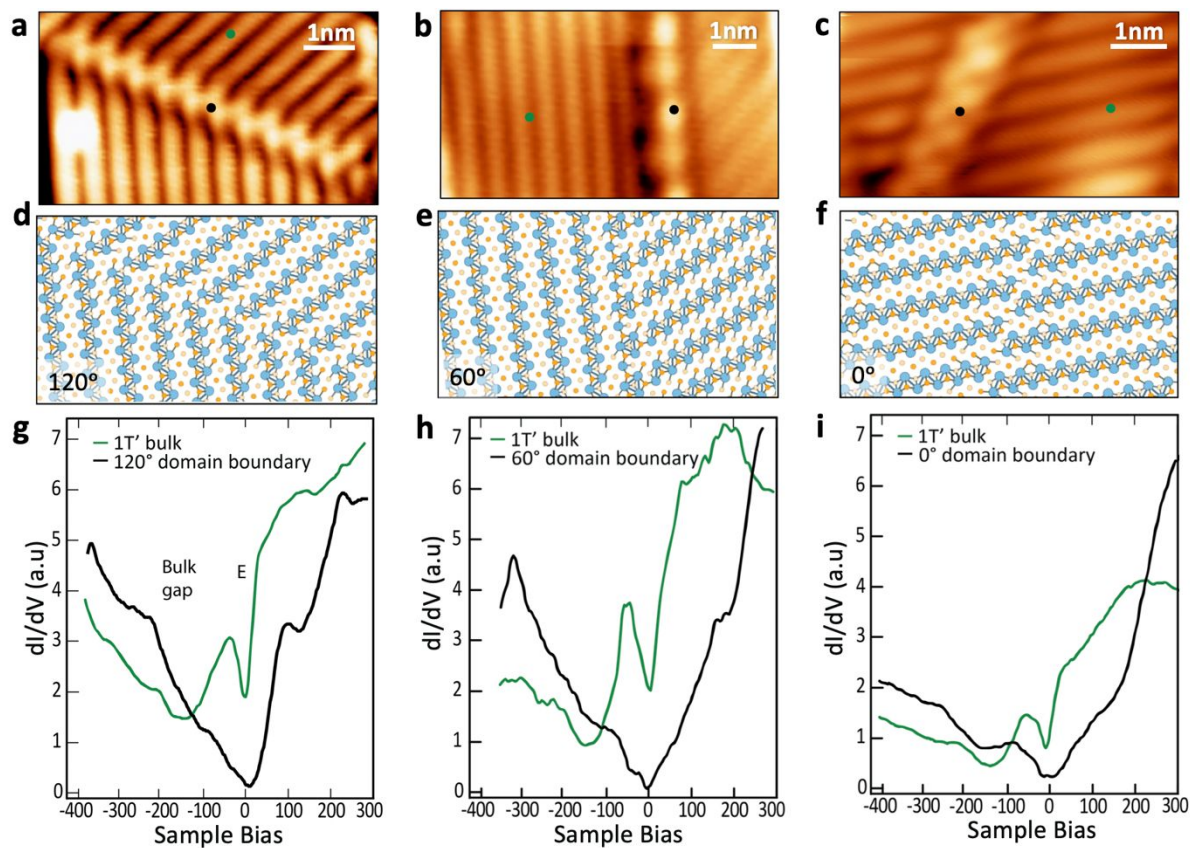


**Figure 2: Structural and electronic properties of 1T'/1T' domain boundaries.** STM images of (a) 120°, (b) 60°, and (c) 0° 1T'/1T' domain boundaries in 1T'-WSe<sub>2</sub> ( $V_s = 1$  V,  $I_t = 10$  pA, standard STM topographs). Relaxed structural models of (d) 120°, (e) 60°, and (f) 0° domain boundaries in 1T'-WSe<sub>2</sub> (calculated using DFT). STM  $dI/dV$  spectroscopy measured at (g) 120°, (h) 60°, and (i) 0° domain boundaries compared to the bulk for single-layer 1T'-WSe<sub>2</sub> (spectroscopy positions marked by black and green dots in (a)-(c)) ( $f = 613.7$  Hz,  $V_{ac} = 4$  mV,  $T = 4.5$  K. Initial tunneling parameters for spectroscopy measurements:  $V_s = -400$  mV,  $I = 100$  pA).

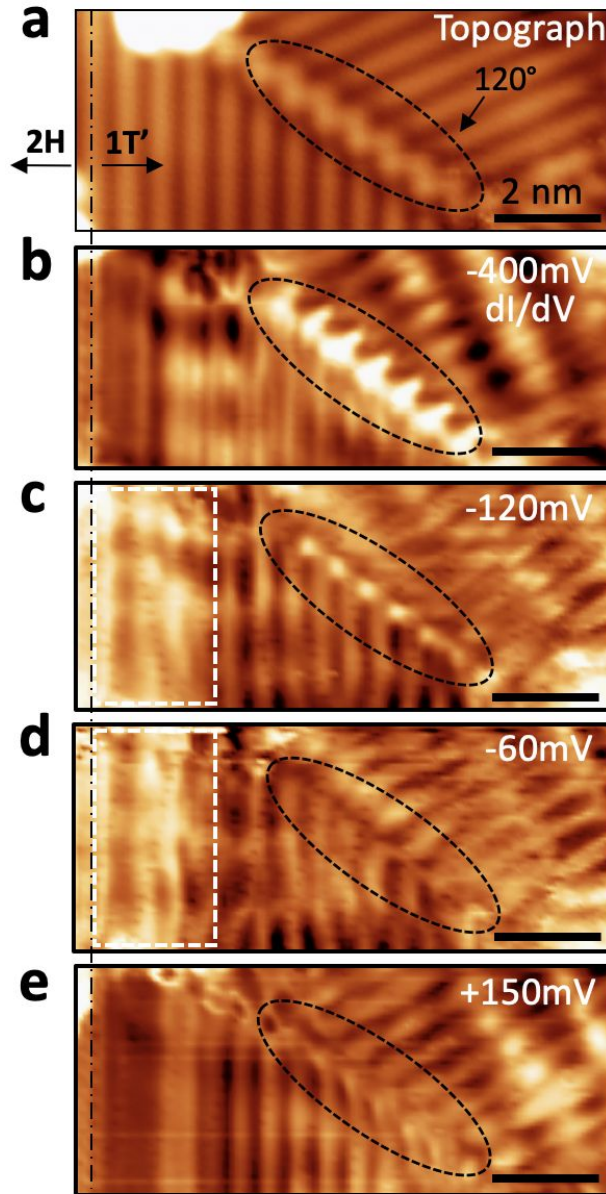


**Figure 3: Comparison of electronic properties of  $120^\circ$   $1T'/1T'$  domain boundary and  $1T'/1H$  boundary coexisting in single-layer  $WSe_2$ .** (a) STM image of a mixed-phase  $WSe_2$  island with a  $120^\circ$   $1T'/1T'$  domain boundary (standard STM topograph). The  $1T'/1H$  interface is marked by a vertical dashed line while the  $1T'/1T'$  interface is outlined by a dashed oval ( $V_s = 1$  V,  $I_t = 10$  pA).  $dI/dV$  maps of the same area are shown for (b)  $V_s = -400$  mV, (c)  $-120$  mV, (d)  $-60$  mV, and (e)  $+150$  mV. Spectroscopy parameters:  $f = 613.7$  Hz,  $V_{ac} = 4$  mV,  $I = 100$  pA,  $T = 4.5$  K. Dashed white box outlines the topologically protected edge-state.



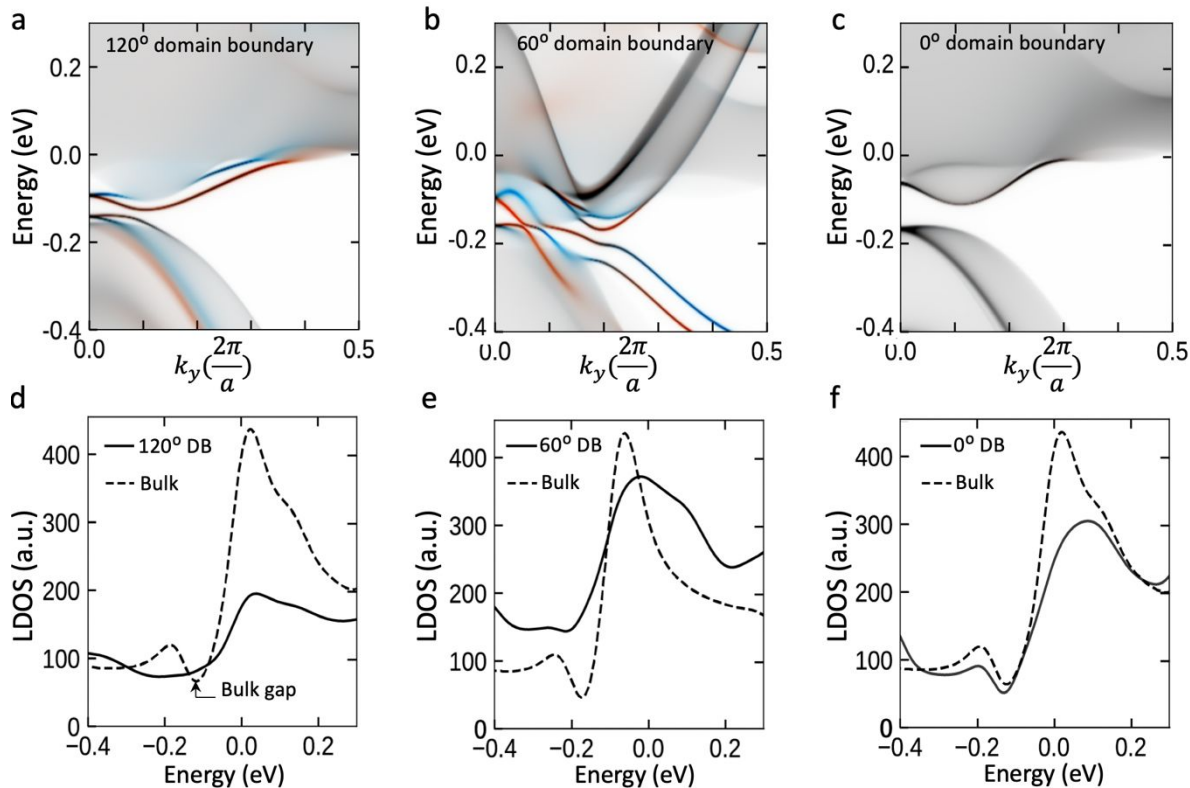


**Figure 4: Calculated Band Structure and Local Density of States of Different 1T'/1T'**

**Domain Boundaries.** Calculated band structure of (a) 120°, (b) 60°, and (c) 0° 1T'/1T' domain boundaries for 1T'-WSe<sub>2</sub> monolayer. Bulk states are grey, spin-polarized interface modes are red and blue. (d-f) Calculated LDOS of top-layer Se atoms at a domain boundary (black solid curve) compared to LDOS in the bulk (black dashed curve) for (d) 120°, (e) 60°, and (f) 0° 1T'/1T' domain boundaries. The Fermi level ( $E = 0$ ) has been shifted to match experimental data (plots presented in (d)-(f) have been convolved with a Gaussian having  $\sigma = 30$  mV to simulate level broadening effects<sup>25</sup>).